Thin Solid Films 772 (2023) 139821

Contents lists available at ScienceDirect

Thin Solid Films

journal homepage: www.elsevier.com/locate/tsf

Electrochemical properties of $CoFe_2O_4$ thin film electrodes prepared by spray pyrolysis

Vidyadevi A. Jundale, Abhijit A. Yadav *

Thin Film Physics Laboratory, Department of Physics, Electronics and Photonics, Rajarshi Shahu Mahavidyalaya (Autonomous), Latur 413512, Maharashtra, India

ARTICLE INFO

Keywords:
Spray pyrolysis
Copper ferrite
Thin films
Supercapacitor
X-ray diffraction
Field emission scanning electron microscopy
Cyclic voltammetry
Electrochemical impedance spectroscopy

ABSTRACT

$CoFe_2O_4$ thin films have been prepared by chemical spray pyrolysis at various substrate temperatures and were characterized for structural, morphological, compositional, optical, electrical and electrochemical properties. X-ray diffraction studies confirmed the spinel cubic phase formation with crystallite size in the range of 15 to 23 nm. Field emission scanning electron microscopy images showed porous spherical granular like surface morphology. Optical bandgap was observed in the range of 2.33 eV to 2.54 eV with direct allowed type transitions. The electrical resistivity measurement confirmed semiconducting behaviour. $CoFe_2O_4$ electrode prepared at 425 °C showed specific capacitance of 543 Fg^{-1} at scan rate of 5 mVs^{-1} from cyclic voltammetry and 575 Fg^{-1} at current density of 0.5 Ag^{-1} from galvanostatic charge-discharge within potential window of 0 V to 0.55 V in aqueous 1 M KOH electrolyte. The specific energy and specific power of $CoFe_2O_4$ thin film prepared at 425 °C were found to be 17.86 $Whkg^{-1}$ and 1108 Wkg^{-1} respectively at current density of 4 Ag^{-1}. $CoFe_2O_4$ thin film prepared at 425 °C exhibited 93.03% retention of its specific capacitance after 1000 cycles at a current density of 1 Ag^{-1}. Electrochemical impedance spectroscopy analysis confirmed the superior electrochemical properties of $CoFe_2O_4$ thin films. The good electrochemical performance suggests use of $CoFe_2O_4$ thin films for supercapacitors.

1. Introduction

The electrochemical storage devices including batteries and capacitors have gained rising attention in research as well as industry during last few decades. Both batteries and capacitors have certain advantages and disadvantages. Batteries have low specific power and high specific energy whereas traditional capacitors have high specific power and low specific energy [1]. As a midway solution amongst batteries and capacitors, with a greater specific capacitance than traditional capacitors and a quicker charge-discharge than batteries, supercapacitors have gained a lot of attention [2]. Supercapacitors show the exceptional features including high specific power, long cycle life and environment-friendliness [3–5].

In literature, RuO_2 is most studied material for supercapacitors. However, due to its scarcity and high cost, it is less appropriate for large-scale applications [6]. Therefore, other transition metal oxides have gained growing attention. Transition metal spinel ferrites such as MFe_2O_4 (M = Ni, Co, Mn, Zn, Cu) and its nanocomposites have been used for energy storage devices and applications [7]. Amongst these, $CoFe_2O_4$ is considered as auspicious material with potentially competitive cycling stability for supercapacitor applications. $CoFe_2O_4$ shows excellent optical, electrical and magnetic properties [8–9]. Furthermore, $CoFe_2O_4$ has good rate stability, strong anisotropy, higher saturation magnetization, coercivity, structural stability and low cost [10–12]. Due to such interesting properties, $CoFe_2O_4$ thin films are used for high temperature gas sensing applications, microwaves, noise filters, transformer cores, energy storage devices, etc. [13]. However, less attention has been paid to the electrochemical properties [14]. Sagu and colleagues [11] have reported $CoFe_2O_4$ thin films in two-electrode configuration with a specific capacitance of 540 μFcm^{-2} and a relaxation time of 174 ms. Kumbhar et al. [15] have obtained specific capacitance of 366 Fg^{-1} in 1 M NaOH electrolyte at scan rate of 5 mVs^{-1} for $CoFe_2O_4$ thin film prepared by chemical route. The effect of substrate temperature on $CoFe_2O_4$ thin films for supercapacitor electrodes produced by pulsed laser deposition has been studied by Nikam and colleagues [16]. For electrodes deposited at RT and 450 °C, respectively, at a current density of 0.5 $mAcm^{-2}$, specific capacitances of approximately 777.4 Fg^{-1} and 258.5 Fg^{-1}, respectively, were achieved. Due to the

* Corresponding author.
E-mail address: aay_physics@yahoo.co.in (A.A. Yadav).

https://doi.org/10.1016/j.tsf.2023.139821
Received 2 May 2022; Received in revised form 29 March 2023; Accepted 29 March 2023
Available online 30 March 2023

growing electroactive surface of $CoFe_2O_4$ and the quick electron and ion transport at the surface, the cyclic stability was raised up to 125% after 1500 cycles [16].

By using a simple drop casting technique, Soam and colleagues [17] have fabricated a bismuth ferrite/graphene nanocomposite. The cyclic voltammetry (CV) test conducted at a scan rate of 10 mVs^{-1} in the potential window of 0–0.9 V revealed a specific capacitance of 9 mF cm^{-2}. It produced 0.5–3.5 kW/kg of specific power and maintained 98% of its capacitance after 1000 cycles and 95% after 5000 cycles. Using the SILAR technique, Raut et al. [18] created thin films with zinc ferrite anchored on multiwalled carbon nanotubes. The inner and outer active surfaces of the hybrid zinc ferrite-carbon nanotube electrode combine to produce a high specific capacity of 217 $mAhg^{-1}$ at 5 mVs^{-1} as a result of the composite electrode's synergy. Additionally, a solid-state symmetric device showed the specific energy of 12.80 Wh kg^{-1} and the specific power of 377.86 W kg^{-1}. The hydrothermal approach was used by Gao and colleagues [19] to prepare $CoFe_2O_4$on the nickel foam. $CoFe_2O_4$ electrode displayed a high capacitance of 1342 Fg^{-1} at 1 Ag^{-1}. The asymmetric supercapacitor has a retention rate of 56% at a current density of 10 Ag^{-1} and an energy density of 55.42 Wh kg^{-1} at a power density of 769.7 W kg^{-1}.

$CoFe_2O_4$ thin films can be prepared by variety of methods including chemical vapour deposition [20], electrodeposition [21], aerosol-assisted chemical vapour deposition [11], coprecipitation [10], Radiofrequency magnetron sputtering [22], wet chemical method [23], hydrothermal [24], spray pyrolysis [25], etc. Amongst these, spray pyrolysis is one of the promising methods used for thin film preparation due to its low cost, flexibility and possibility for large area deposition [26–28]. In the present study, $CoFe_2O_4$ thin films have been prepared by spray pyrolysis at various substrate temperatures, the effect of substrate temperatures on structural, morphological, compositional, optical, electrical and electrochemical properties have been studied.

2. Experimental

$CoFe_2O_4$ thin films have been prepared onto ultrasonically cleaned amorphous glass (7.5 cm × 2.5 cm × 0.13 cm) and fluorine doped tin oxide (FTO) coated glass substrates (~7Ω cm^2) using chemical spray pyrolysis method. For the preparation of $CoFe_2O_4$ thin films, all the used chemicals were AR grade. For each deposition, freshly prepared 5 ml of 0.15 M $Co(NO_3)_2{\cdot}6H_2O$ and 10 ml of 0.15 M $Fe(NO_3)_3{\cdot}9H_2O$ were mixed thoroughly by stirring for 15 min. To this 15 ml solution, 15 ml of ethanol was added to make final spraying solution 30 ml. Finally, 30 ml solution was sprayed onto preheated glass and FTO coated conducting glass substrates. During the deposition experiments, the substrate temperature was varied from 375 °C to 475 °C in 25 °C increments by keeping all other parameters constant at their optimized values namely spray rate; 3–4 $mlmin^{-1}$, substrate to nozzle distance 30 cm; and air as carrier gas with pressure 176.5 kPa. In each deposition, 2 samples of $CoFe_2O_4$ thin film on amorphous glass substrates (7.5 cm × 2.5 cm × 0.13 cm) and 4 samples of $CoFe_2O_4$ thin film on FTO substrates (1 cm × 1 cm) were obtained.

Structural properties and phase identification of $CoFe_2O_4$ thin films (1 cm × 1 cm) were studied by X-ray diffraction (XRD) using the X-ray diffractometer (Philips model PW-1710) with Cu-Kα radiation (λ = 1.5406 Å). Field emission scanning electron microscope (FESEM) at operating voltage 10–20 kV (Model No-S-4800 Hitachi high technologies corporation, Japan) was used to study the surface morphology of $CoFe_2O_4$ thin films. Energy-dispersive X-ray spectroscopy (EDX) (Model No-X flash 5030 detector, Bruker AXS Gmbh, Germany) was used to determine the elemental analysis and compositions of $CoFe_2O_4$ thin films. To study the optical properties, the optical absorption spectra of $CoFe_2O_4$ thin films was recorded using UV–Vis spectrophotometer (SHIMADZU-1700) within wavelength range of 400 to 900 nm. To determine the electrical resistivity of $CoFe_2O_4$ thin films, direct current (DC) two-point probe method was used. Electrochemical performances were studied in the standard three-electrode cell on a CHI-608D (CH Instruments, USA). For electrochemical performance, the $CoFe_2O_4$ thin films as a working electrode, platinum (Pt) wire as counter electrode and Ag/AgCl as a reference electrode were used. Using CHI instrument, analysis of CV has been carried out at different scan rate within potential range of 0.0 to 0.55 V in 1 M KOH aqueous electrolyte, galvanostatic charge-discharge (GCD) analysis was used to study the charge-discharge behaviour of the $CoFe_2O_4$ electrodes. Using AC signal multi-frequency electrochemical impedance spectroscopy measurement (EIS) was carried out in the frequency range from 1 Hz to 1 kHz.

3. Results and discussion

3.1. Chemical reaction

In spray pyrolysis, the precursor solution is pulverized by means of air. The fine droplets of the precursor solution are sprayed onto preheated substrates. The thermal decomposition of fine droplets of Co $(NO_3)_2{\cdot}6H_2O$ and $Fe(NO_3)_3{\cdot}9H_2O$ solution results into the formation of dark grey to black $CoFe_2O_4$ thin films and volatile products at the temperature of deposition. Fig. 1 shows the actual photograph of $CoFe_2O_4$ thin films prepared by spray pyrolysis at various substrate temperatures.

A simple reaction mechanism for formation of $CoFe_2O_4$ thin films can be given as;

The $Co(NO_3)_2{\cdot}6H_2O$ in aqueous solution decomposes to form Co $(OH)_2$ as [29];

$$Co(NO_3)_26H_2O + 2H_2O \rightarrow Co(OH)_2 + 2HNO_3 + 6H_2O \quad (1)$$

The $Fe(NO_3)_3{\cdot}9H_2O$ in aqueous solution decomposes to form Fe $(OH)_3$ as [29];

$$2Fe(NO_3)_39H_2O + 6H_2O \rightarrow 2Fe(OH)_3 + 6HNO_3 + 18H_2O \quad (2)$$

The aqueous solution containing $Co(OH)_2$ and $Fe(OH)_3$ decomposes pyrolytically to form the spinel cobalt ferrite as [26]:

$$Co(OH)_2 + 2Fe(OH)_3 \rightarrow CoFe_2O_4 + 4H_2O\uparrow \quad (3)$$

Simillar type of reaction mechanism has been previously reported by Karthigayan et al. [29] for $CoFe_2O_4$ thin films by spray pyrolysis.

3.2. Film thickness

Film thickness is the significant parameter that alters the material properties due to its surface phenomenon. Apparent film thicknesses of $CoFe_2O_4$ thin films prepared by spray pyrolysis at various substrate temperatures were determined by gravimetric weight difference method using sensitive microbalance (Least count = 0.01 mg) [30].

$$t = \frac{\Delta m}{A \times \rho} \quad (4)$$

where, 't' is the thickness of the $CoFe_2O_4$ thin film, 'Δm' is the mass difference (the difference between the weight of the film before the deposition and after the deposition), 'ρ' is the density of the material assuming the bulk density of $CoFe_2O_4$ of ρ = 5.29 gcm^{-3} [31] and 'A' is the area of $CoFe_2O_4$ thin films. The apparent film thicknesses were found to be 417 nm, 646 nm, 774 nm, 728 nm and 600 nm for $CoFe_2O_4$ thin films prepared by spray pyrolysis at substrate temperatures of 375 °C, 400 °C, 425 °C, 450 °C and 475 °C respectively.

Fig. 2 shows the variation of apparent film thickness with substrate temperature for $CoFe_2O_4$ thin films prepared by spray pyrolysis. Initially as substrate temperature increases from 375 °C, the apparent film thickness increases form 417 nm to 774 nm for substrate temperature of 425 °C and thereafter with increase in substrate temperature apparent film thickness decreases. The effect of substrate temperature on apparent film thickness can be explained as follows: the lower substrate

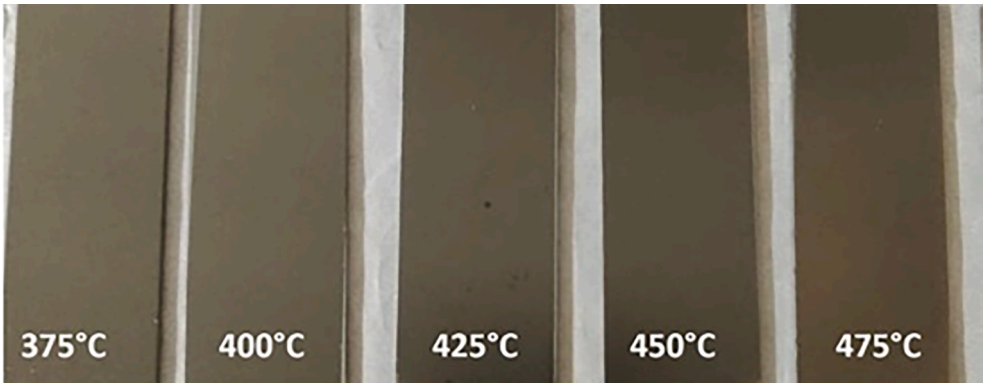

Fig. 1. Photograph of $CoFe_2O_4$ thin films prepared by spray pyrolysis at various substrate temperatures.

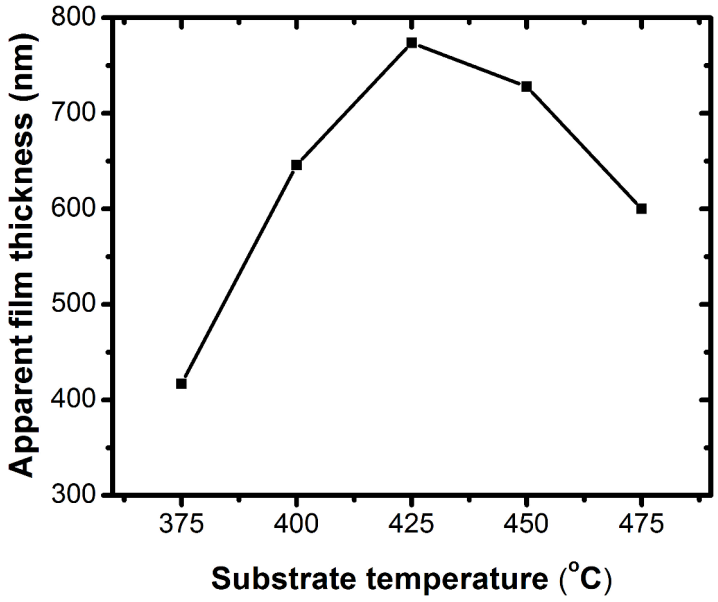

Fig. 2. Variation of apparent film thickness with substrate temperature for $CoFe_2O_4$ thin films prepared by spray pyrolysis.

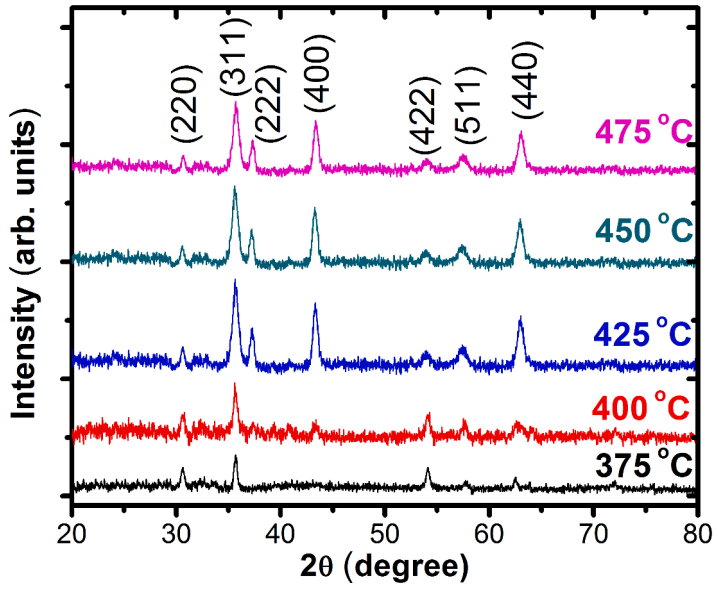

Fig. 3. XRD plots of $CoFe_2O_4$ thin films prepared by spray pyrolysis at various substrate temperatures.

temperature (375 °C) is not enough for the decomposition of the nitrates present in the solution, resulting in lower apparent film thickness of $CoFe_2O_4$ thin films. At a particular substrate temperature (425 °C), decomposition of the ions occurs at optimum level confirming the terminal apparent film thickness being accomplished. At higher substrate temperature i.e. beyond the optimum substrate temperature of 425 °C, the decrease in apparent film thickness is due to a reduction in the deposition rate of the initial specimens with rise in substrate temperature. Similar behaviour was earlier reported for NiO thin films by spray pyrolysis [32].

3.3. XRD

Structural study of $CoFe_2O_4$ thin films prepared by spray pyrolysis at various substrate temperatures was carried out using XRD with CuKα radiation and 2θ in the range of 20°−80° Fig. 3 shows the XRD patterns of $CoFe_2O_4$ thin films prepared by spray pyrolysis at substrate temperatures 375 °C, 400 °C, 425 °C, 450 °C and 475 °C respectively. From XRD pattern, the intense peaks were observed at 2θ around 30.63°, 35.4°, 37.1°, 43.1°, 53.4°, 57.2° and 62.6° with corresponding planes (220), (311), (222), (400), (422), (511) and (440) respectively. The matching of standard and calculated 'd' values confirm the spinel cubic phase formation with the space group of Fd-3 m (S.G. number 227) of $CoFe_2O_4$ (JCPDS card no. 22–1086) [33]. $CoFe_2O_4$ phase has an inverse spinel structure with Co^{2+} ion occupying half of the octahedral (B) sites, i.e. $Fe^{3+}(Co^{2+}Fe^{3+})O_4$. The XRD broadening lines show that $CoFe_2O_4$ thin film is nanocrystalline.

As seen from the figure, peak intensity is substrate temperature dependant. The peak intensity increases with increasing substrate temperature attain maximum at 425 °C and decreases thereafter. At 425 °C, the increased peak intensity (311) indicates optimum growth for $CoFe_2O_4$ thin films [34]. In addition, it has been witnessed that there is an evolution of the peak from the (222) diffraction plane and decrease in peak intensities from the (440) diffraction plane as the substrate temperature increased above 425 °C. This might be due to fact that the substrate temperature affected cation distribution for both tetrahedral and octahedral sites. The cations on tetrahedral sites are most sensitive to the intensities corresponding to the (220) and (422) planes, while the cations on octahedral sites are most sensitive to the intensities corresponding to the (222) plane. Simillar results have been reported by Purnama et al. [35] for cobalt ferrite nanoparticles.

The crystallite sizes of $CoFe_2O_4$ thin films prepared by spray pyrolysis at various substrate temperatures were estimated from Debye-Scherrer formula [36]

$$D = \frac{0.9\lambda}{\beta cos\theta} \tag{5}$$

where, D; average crystallite size, λ; X-ray wavelength, β; full width at half the maxima, and θ; Bragg's angle. The determined values of crystallite sizes of $CoFe_2O_4$ films at various substrate temperatures are reported in Table 1, which indicates that crystallite size 23 nm was maximum for $CoFe_2O_4$ films prepared at substrate temperature of 425 °C. The lattice parameter 'a' of $CoFe_2O_4$ films for (311) plane was determined using the standard relation [37].

$$a = d \times \sqrt{h^2 + k^2 + l^2} \tag{6}$$

The calculated average lattice parameter $a = 8.3226$ Å is close to standard JCPDS data card value $a = 8.3910$ Å (JCPDS card no. 22–1086) [33].

3.4. Field emission scanning electron microscopy

Fig. 4 shows the surface micrographs (magnification ×200 k) of $CoFe_2O_4$ thin films prepared by spray pyrolysis at various substrate temperatures. From micrographs, it is apparent that $CoFe_2O_4$ thin films showed a homogenous crack-free spherical nano grain type morphology. The spherical grain morphology is mostly observed in metal oxide thin films. The $CoFe_2O_4$ thin film prepared at 375 °C depicts micrograph with smaller grains and denser surface than that of other samples. The $CoFe_2O_4$ thin film prepared at substrate temperature of 400 °C shows the nucleation of small grain-like nanoparticles. Fig. 4(c) shows image of uniformly dispersed agglomerated spherical $CoFe_2O_4$ nanoparticles ranging in size 40–80 nm for $CoFe_2O_4$ thin film prepared at substrate temperature of 425 °C. The porous morphology observed at substrate temperature of 425 °C is suitable for supercapacitor applications [38]. As the substrate temperature increases to 450 °C grain like surface morphology becomes compact, dense and agglomerated. Dense and compact surface morphology diversely affects electrochemical active sites resulting in the reduction of rate of intercalation/deintercalation of the electrolyte ions. At 475 °C, grain like surface morphology becomes more compact and highly dense as compared to 450 °C. It reduces the porosity and leads to reduction in electrochemical active sites and further decreases the electrochemical performance. Such a spherical nanostructure grain like surface morphology of $CoFe_2O_4$ is previously reported by Feng et al. [39] for $CoFe_2O_4/NiFe_2O_4$ nanocomposites prepared via a facile hydrothermal method and Rao and coworkers [40] for $CoFe_2O_4$ thin films prepared via sol-gel method.

Table 1
Structural parameters for $CoFe_2O_4$ thin films prepared by spray pyrolysis at various substrate temperatures.

Substrate Temp. (°C)	2θ (°)	d (Å) Obs.	d (Å) Std.	hkl	a (Å)	D (nm)
375	30.63	2.916	2.976	220	8.312	15
	35.69	2.513	2.533	311		
	54.13	1.693	1.714	422		
	57.72	1.596	1.614	511		
	62.55	1.484	1.482	440		
400	30.77	2.903	2.976	220	8.309	21
	35.60	2.519	2.533	311		
	43.38	2.084	2.097	400		
	54.28	1.688	1.714	422		
	57.71	1.596	1.614	511		
	62.59	1.483	1.482	440		
425	30.58	2.921	2.976	220	8.331	23
	35.63	2.517	2.533	311		
	37.20	2.415	2.421	222		
	43.31	2.087	2.097	400		
	53.87	1.700	1.714	422		
	57.40	1.604	1.614	511		
	63.02	1.474	1.482	440		
450	30.55	2.923	2976	220	8.338	20
	35.59	2.520	2.533	311		
	37.14	2.418	2.421	222		
	43.28	2.088	2.097	400		
	53.84	1.701	1.714	422		
	57.37	1.605	1.614	511		
	62.98	1.474	1.482	440		
475	30.62	2.917	2.976	220	8.323	17
	35.68	2.514	2.533	311		
	37.24	2.412	2.421	222		
	43.34	2.086	2.097	400		
	53.92	1.699	1.714	422		
	57.46	1.602	1.614	511		
	63.06	1.472	1.482	440		

2θ; Bragg's angle, d; interplanar spacing, hkl; miller indices, a; lattice constant, D; crystallite size.

3.5. Energy-dispersive X-ray spectroscopy

The chemical composition and stoichiometry of $CoFe_2O_4$ thin films were analysed using EDX method. Table 2 shows the compositional analysis of $CoFe_2O_4$ thin films prepared by spray pyrolysis at various substrate temperatures. The presence of cobalt, iron and oxygen confirms the spray deposition of $CoFe_2O_4$. The $CoFe_2O_4$ thin film prepared at 425 °C is nearly stoichiometric whereas the $CoFe_2O_4$ films prepared

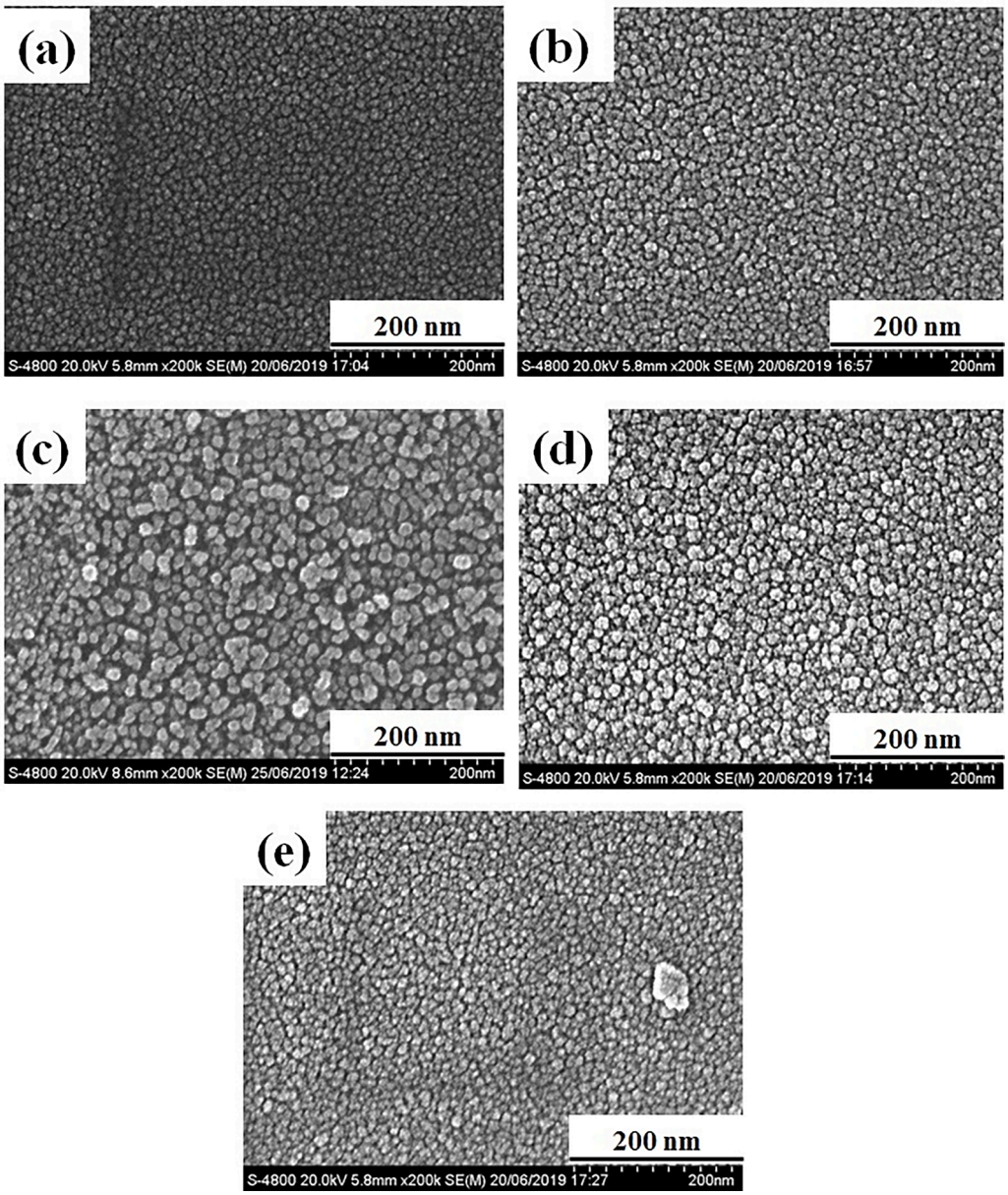

Fig. 4. FESEM images (magnification ×200 k) of $CoFe_2O_4$ thin films prepared by spray pyrolysis at substrate temperatures of (a) 375 °C, (b) 400 °C, (c) 425 °C, (d) 450 °C and (e) 475 °C respectively.

Table 2
The elemental composition of $CoFe_2O_4$ thin films prepared by spray pyrolysis.

Substrate Temp. (°C)	Atomic percentage of $CoFe_2O_4$ thin films (%)		
	Co	Fe	O
375	13	23	64
400	13	27	60
425	14	28	58
450	16	29	55
475	15	28	57

above substrate temperature 425 °C are slightly cobalt rich.

3.6. Optical

The UV–Visible absorption spectra of $CoFe_2O_4$ thin films prepared by spray pyrolysis at various substrate temperatures were recorded at room temperature in the wavelength range of 400–900 nm and is shown in Fig. 5(a). All films showed a high coefficient of absorption in the range of 10^4 cm^{-1}. The optical absorption spectra were used to determine the bandgap energy of the $CoFe_2O_4$ thin films using the Tauc's relation [41].

$$\alpha = \frac{A(Eg - h\nu)^n}{h\nu} \quad (7)$$

where α; absorption coefficient, A; is an energy independent constant and Eg; stands for bandgap, hυ; incident photon energy. The exponent $n = 1/2$ or 2 are allowed direct bandgap or indirect bandgap transitions respectively. Fig. 5(b) shows the plot of $(\alpha h\upsilon)^2$ verses hυ for $CoFe_2O_4$ thin films prepared by spray pyrolysis at various substrate temperatures. The nature of plot suggests direct allowed type transition for $CoFe_2O_4$ thin films [42]. The bandgap energy (Eg) was estimated by assuming a direct transition between valence and conduction bands and by extrapolating the portion of the $(\alpha h\upsilon)^2$ verses hυ graph to $\alpha h\upsilon = 0$ on energy (hυ) axis. These bandgap values are given in Table 3. Fig. 5(c) indicates the variation of bandgap energy with substrate temperature for $CoFe_2O_4$ thin films prepared by spray pyrolysis. The bandgap energies of $CoFe_2O_4$ thin films are in the range of 2.33 to 2.54 eV. These values are

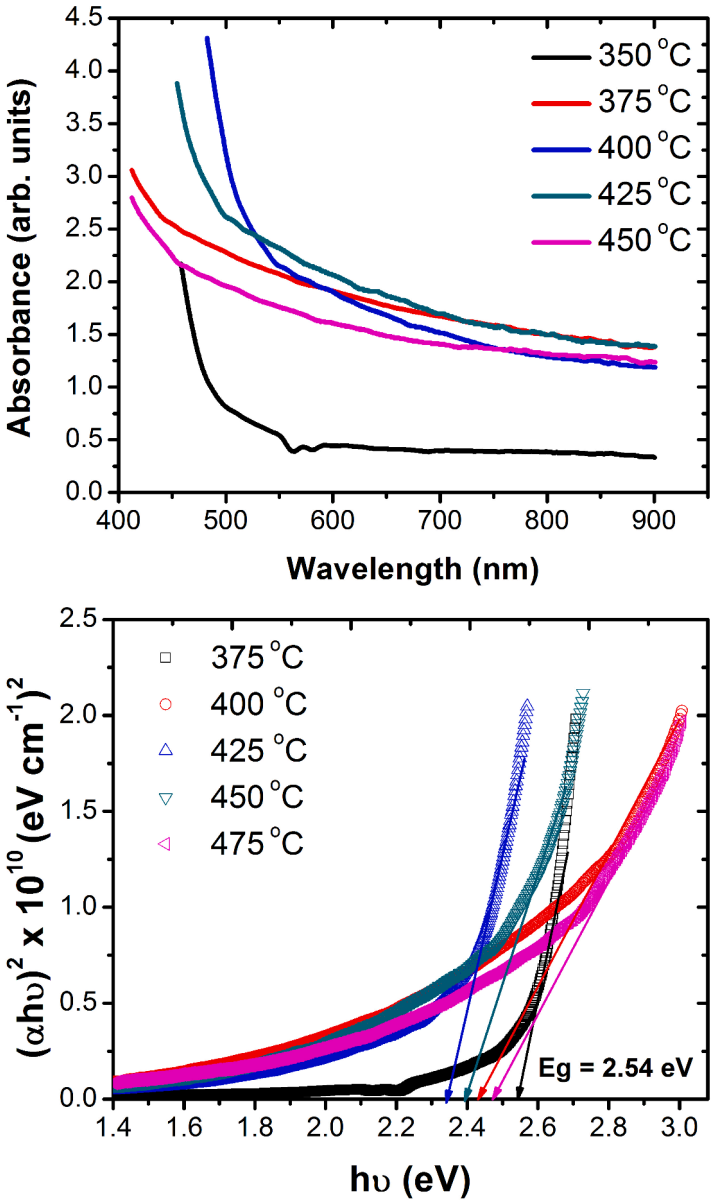

Fig. 5. (a) absorbance spectra, **(b)** Plots $(\alpha h\upsilon)^2$ versus $h\upsilon$ and **(c)** Variation of bandgap energy with substrate temperature for $CoFe_2O_4$ thin films prepared by spray pyrolysis.

close to the bandgap energy of 2.273 eV reported by Yuliantika and colleagues [43] for cobalt ferrite nanoparticles. The bandgap of $CoFe_2O_4$ is due to d to d transition. The existence of crystal field separates d level into e_g and t_{2g} levels and the energy width are higher for octahedral site than tetrahedral site. The variation of bandgap of $CoFe_2O_4$ with increase in substrate temperature seems to be due to the redistribution of Co^{2+}on the octahedral and tetrahedral sites with increase in substrate temperature. In spinel $CoFe_2O_4$ thin films, if there is a redistribution of Co^{2+} between octahedral site and tetrahedral site then, this can affect the observed bandgap. In the present case, it seems that the substrate temperature causes shifting of Co^{2+} from octahedral site to tetrahedral site resulting in the decrease in bandgap of $CoFe_2O_4$ thin films [44]. Above 425 °C substrate temperature, the bandgap energy increases from 2.33 eV to 2.47 eV for substrate temperature of 425 °C. The similar kind of variation in the bandgap energy is reported by Loan and coworkers [45] for $CoFe_2O_4$ nanomaterials.

The variation in the bandgap can also be related with crystallize size variation (Table 1). It has been reported that, the bandgap energy of the nanomaterials is larger than their micron-sized materials [46]. The quantum mechanical effects of the small crystallites are thought to be the cause of the bandgap widening of nanomaterials. Generally, the ferrite materials whose bandgap energy is less than 3 eV shows spinel structure of the materials [47]. Spinel structure of the iron and cobalt provides good electronic conductivity and more active sites helpful for improvement electrochemical performance of the $CoFe_2O_4$ electrodes [48].

3.7. Electrical resistivity

Fig. 6 shows the variation of logarithm of resistivity with inverse of absolute temperature (1000/T) for $CoFe_2O_4$ thin films prepared by spray pyrolysis at various substrate temperatures. As the operating temperature used for measurement increases the electrical resistivity of all $CoFe_2O_4$ thin films decreases showing a typical semiconducting behaviour. This behaviour is due to the thermally activated charge carriers instead of generation of carriers [49,50].

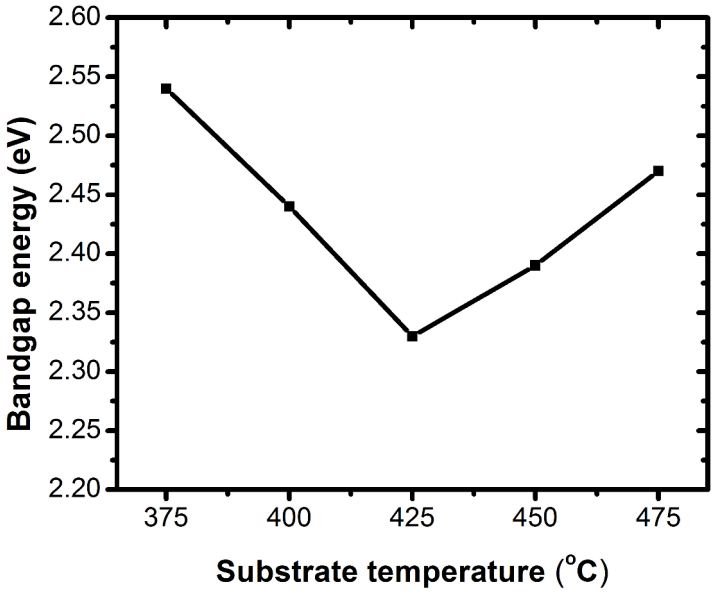

Fig. 5. (*continued*).

Table 3
Optical and electrical properties of $CoFe_2O_4$ thin films prepared by spray pyrolysis at various substrate temperatures (LT; low temperature, HT; High temperature).

Ts (°C)	Eg (eV)	Electrical resistivity (Ω-cm)		Ea (eV)	
		300 K ($\times 10^4$)	500 K ($\times 10^2$)	L.T.	H.T.
375	2.54	852	7.244	0.021	0.066
400	2.44	56.20	0.765	0.022	0.055
425	2.33	2.82	0.093	0.008	0.051
450	2.39	13.80	0.251	0.016	0.059
475	2.47	282	2.589	0.021	0.056

Ts; Substrate Temperature, Eg; Band gap energy, Ea; Activation energy, L.T; Low temperature, H.T.; High temperature.

Table 3 shows the electrical resistivities of $CoFe_2O_4$ thin films at 300 K and 500 K. At 300 K, minimum electrical resistivity was found to be 2.82×10^4 Ωcm for $CoFe_2O_4$ thin film prepared at 425 °C which is lower than the reported value of 2.59×10^6 Ωcm by Gul and Maqsood [51] for cobalt ferrites prepared by sol-gel method. It has been observed that as substrate temperature increases upto 425 °C the electrical resistivity of $CoFe_2O_4$ thin film decreases. The decrease in resistivity is due to the increase in both carrier concentration and carrier mobility of $CoFe_2O_4$ thin films with increase in substrate temperature upto 425 °C. Also the crystallite size observed at 425 °C is maximum; the crystallites are comparatively larger and allow the carriers freely in the lattice leading to decrease in electrical resistivity. For substrate temperatures above 425 °C, the electrical resistivity increases with substrate temperature because carrier concentration is the dominant factor; carrier concentration becomes lower due to decreased crystallite size at higher substrate temperature, leading to higher electrical resistivity [50].

The activation energies of $CoFe_2O_4$ thin films prepared by spray pyrolysis at various substrate temperatures were determined by using the Arrhenius equation [51].

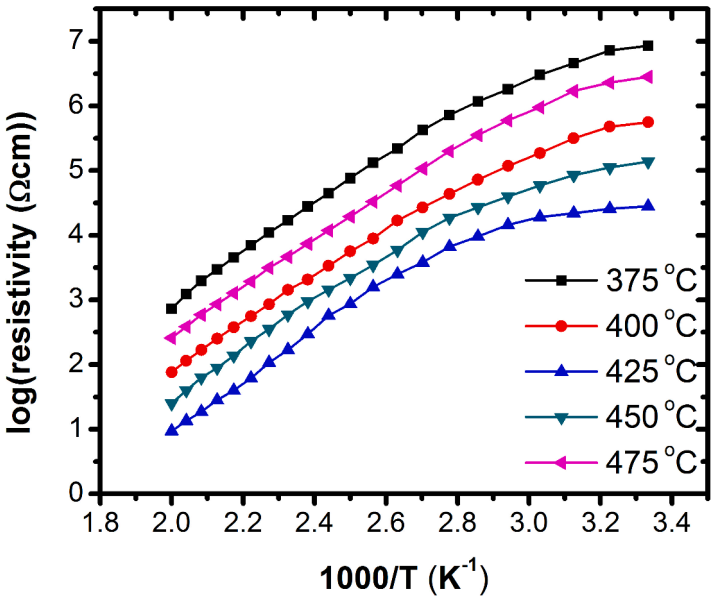

Fig. 6. The variation of logarithm of resistivity with inverse of absolute temperature (1000/T) for $CoFe_2O_4$ thin films prepared by spray pyrolysis.

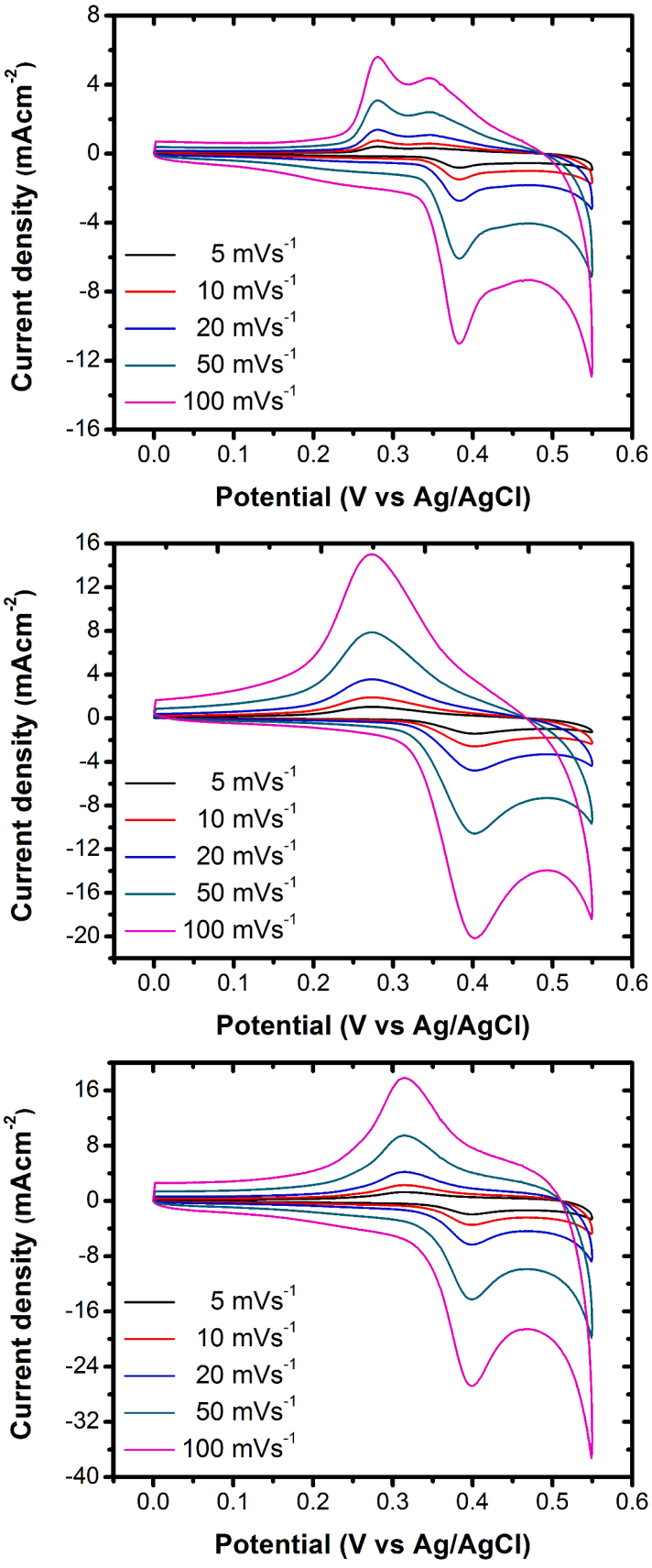

Fig. 7. CV Plots at scan rates of 5 to 100 mVs^{-1} for $CoFe_2O_4$ thin films prepared by spray pyrolysis at various substrate temperatures (a) 375 °C, (b) 400 °C, (c) 425 °C, (d) 450 °C and (e) 475 °C respectively.

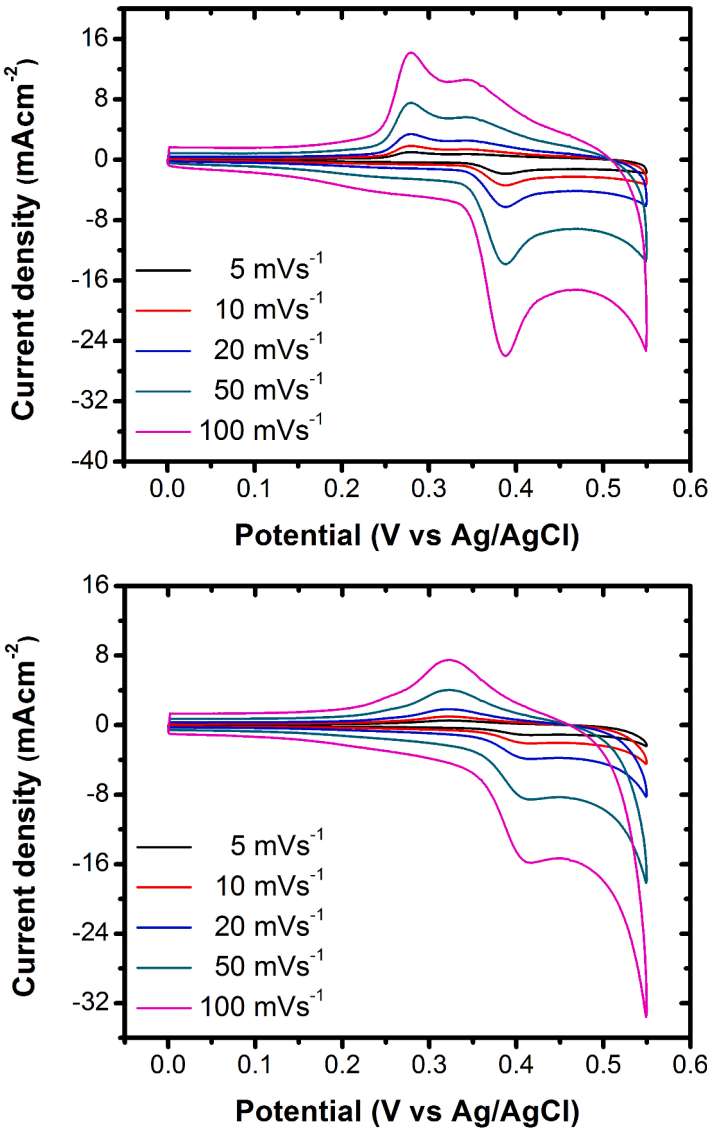

Fig. 7. (*continued*).

$$Resistivity = \rho_0 exp\left(\frac{-E_a}{kT}\right) \quad (8)$$

where ρ_0 represent the resistivity of the semiconducting material and the resistivity constant, respectively, k is the Boltzmann constant, and T indicates the absolute temperature. The slope of the plot of the logarithm of resistivity versus 1000/T is used to determine the thermal activation energy. The activation energies were found to be 0.051–0.066 eV and 0.008–0.022 eV in high temperature and low temperature regions respectively and are mentioned in Table 3. In ferrites, electrical resistivity depends on various parameters such as crystal structure, grain size, chemical composition and number of Fe^{+2} ions present in the octahedral B-site which plays a vital role in the $Fe^{+2} \leftrightarrow Fe^{+3}$ exchange interactions [52,53].

3.8. Electrochemical characterization

3.8.1. CV

The CV study of $CoFe_2O_4$ thin films prepared by spray pyrolysis at various substrate temperatures was performed by using conventional three-electrode configuration in 1 M KOH electrolyte at different scan rates from 5 mVs^{-1} to 100 mVs^{-1}. Fig. 7 (a-e) shows the CV plots at scan rates of 5 mVs^{-1} to 100 mVs^{-1} for $CoFe_2O_4$ thin films. The CV curves for all samples were symmetric with two redox peaks indicating pseudo-capacitive behaviour [54]. Fig. 8(a) shows the CV plots of $CoFe_2O_4$ thin films prepared by spray pyrolysis at various substrate temperatures in the 1 M KOH electrolyte at scan rate of 10 mVs^{-1}. It has been observed that as substrate temperature increases the area under the CV curves also increases upto 425 °C and decreases thereafter.

Specific capacitances at different scan rates for $CoFe_2O_4$ thin films were determined by using the equation [55],

$$C_{sp} = \frac{1}{mv(Vc - Va)} \int_{Va}^{Vc} I(V)dV \quad (9)$$

where, C_{sp}; the specific capacitance, (Vc-Va); operational potential window, I; current of film, and m; mass of $CoFe_2O_4$ active electrode material deposited on 1 cm^2 surface of FTO coated glass substrate.

Fig. 8(b) shows the variation of specific capacitance with scan rate for $CoFe_2O_4$ thin films prepared by spray pyrolysis at various substrate temperatures. It has been observed that as substrate temperature increases from 375 °C to 425 °C, specific capacitance increases. For further increase in substrate temperature above 425 °C the specific capacitance decreases. This behaviour is due to the variation in the surface

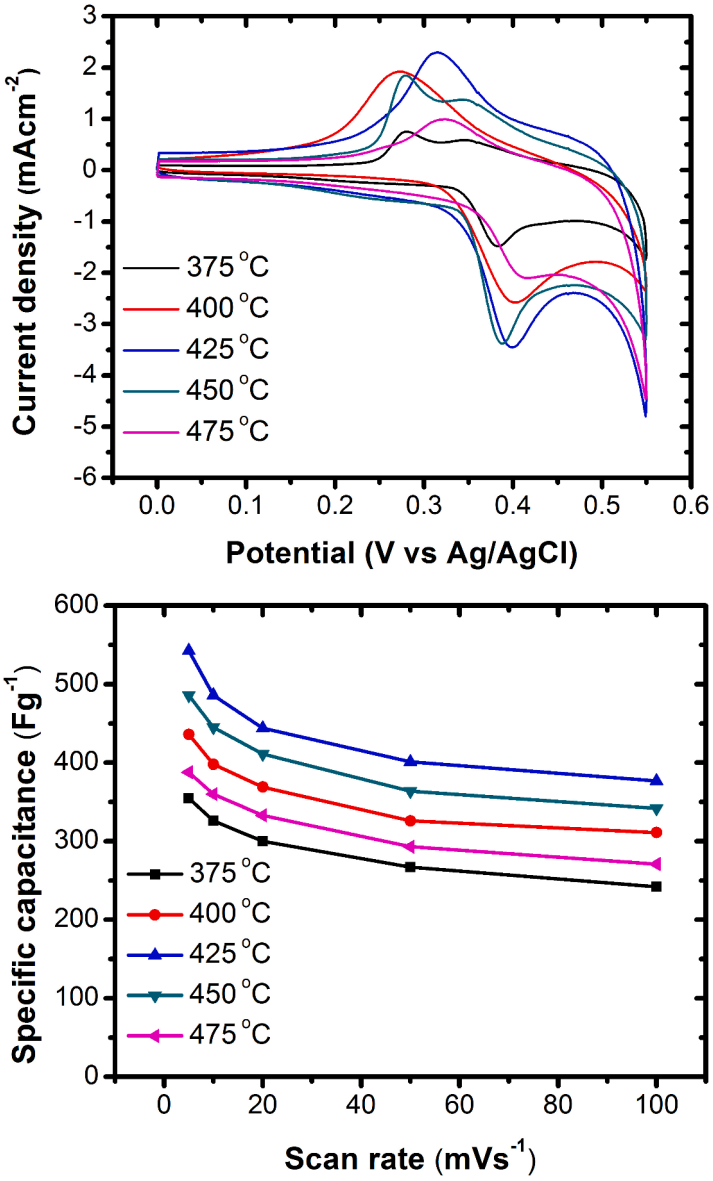

Fig. 8. (a) CV plots at scan rate of 10 mVs^{-1} and (b) variation of specific capacitance with scan rate for $CoFe_2O_4$ thin films prepared by spray pyrolysis at various substrate temperatures.

morphology of $CoFe_2O_4$ thin films. Maximum specific capacitance of 543 Fg^{-1} at scan rate of 5 mVs^{-1} within potential window 0 to 0.55 V was observed for $CoFe_2O_4$ thin films prepared by spray pyrolysis at substrate temperature 425 °C. At 425 °C, surface morphology of $CoFe_2O_4$ thin film was porous grain like interlocked nanostructure which provided more active sites for electrochemical reaction. Hence, the electrochemical performance improves [56] or it may be due to easy ionic intercalation and good crystallinity with supporting morphology as seen from XRD and FESEM results. The obtained specific capacitance is better than specific capacitance of 142 Fg^{-1} at 2 mVs^{-1} reported by Lv et al. [54] for chemically synthesized $CoFe_2O_4$ nanoparticles, 195 Fg^{-1} at 1 mVs^{-1} reported by Sankar and coworkers [57] for $CoFe_2O_4$ nanoparticles. The obtained results are also superior to reported value of 366 Fg^{-1} at 5 mVs^{-1} by Kumbhar and coworkers [15] for $CoFe_2O_4$ thin film prepared by chemical route.

Also from Fig. 8(b), it is seen that as scan rate increases specific capacitance decreases. This is because at higher scan rate the outer pores present in the active electrode material get recovered by the ions in the material or motion of the ions in the electrode materials may be quick, simultaneously diffusion of ions in the electrolyte are slow [58]. At lower scan rate, inner and outer pore of electrode material are available for ion propagation or ion diffusion [59].

3.8.2. GCD

Fig. 9(a-e) shows the GCD curves of $CoFe_2O_4$ thin films prepared by spray pyrolysis at various substrate temperatures, which are nonline ar and symmetric. Liu and coworkers [60] previously reported such nonlinear and symmetric behaviour for $CoFe_2O_4$ thin films in supercapacitor applications. The nonlinear nature of the discharge curve indicates pseudocapacitive behaviour [61], and can be attributed to the electrochemical adsorption-desorption reaction between the active electrode and electrolyte [62]. As substrate temperature increases from 375 °C to 475 °C discharge time for various current densities increases upto 425 °C and decreases thereafter. At substrate temperature of 425 °C, the porous surface morphology of $CoFe_2O_4$ thin film increases the rate of redox reaction allowing more interaction with the electrolyte resulting in rise in discharge time. Fig. 10(a) shows the GCD curves at current density of 1 Ag^{-1} for $CoFe_2O_4$ thin film electrodes prepared by spray pyrolysis at various substrate temperatures. The specific capacitance (Cs), specific energy (SE) and specific power (SP) of $CoFe_2O_4$ thin

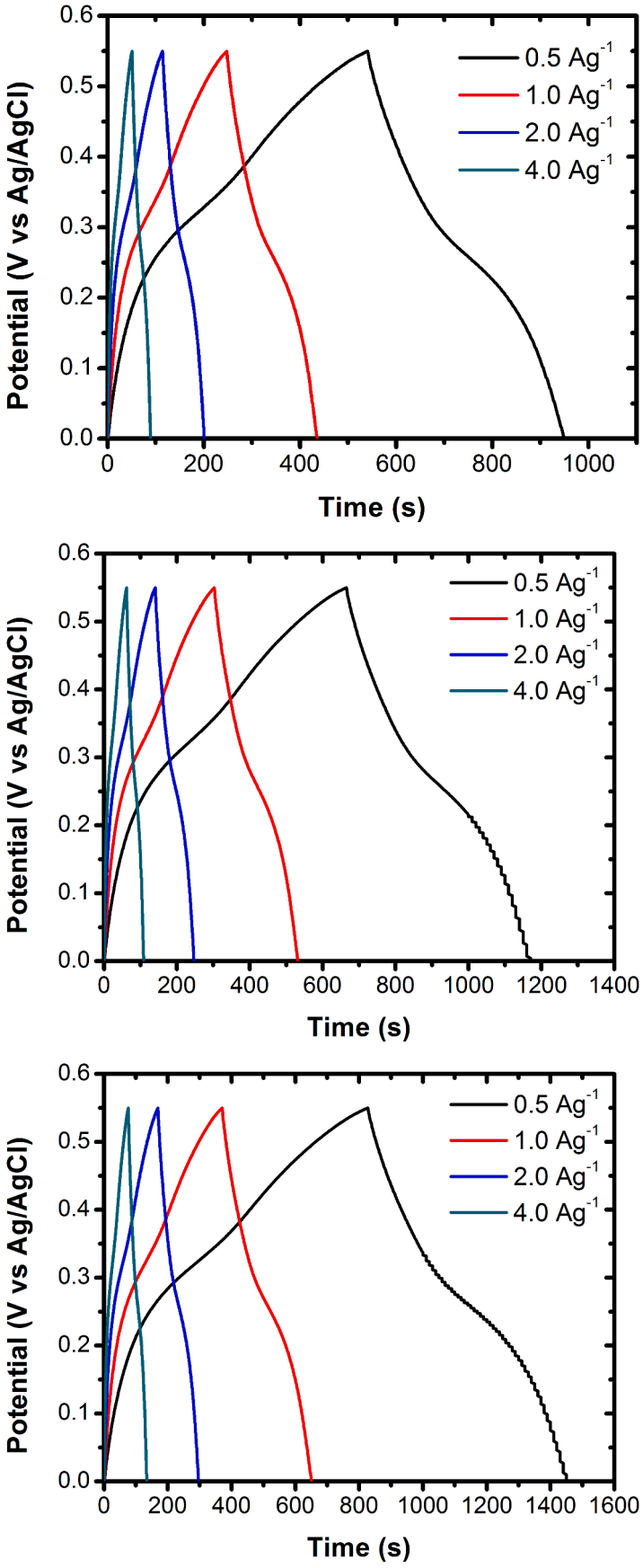

Fig. 9. GCD curves at different current densities for $CoFe_2O_4$ thin films prepared by spray pyrolysis at substrate temperatures of (a) 375 °C, (b) 400 °C, (c) 425 °C, (d) 450 °C and (e) 475 °C respectively.

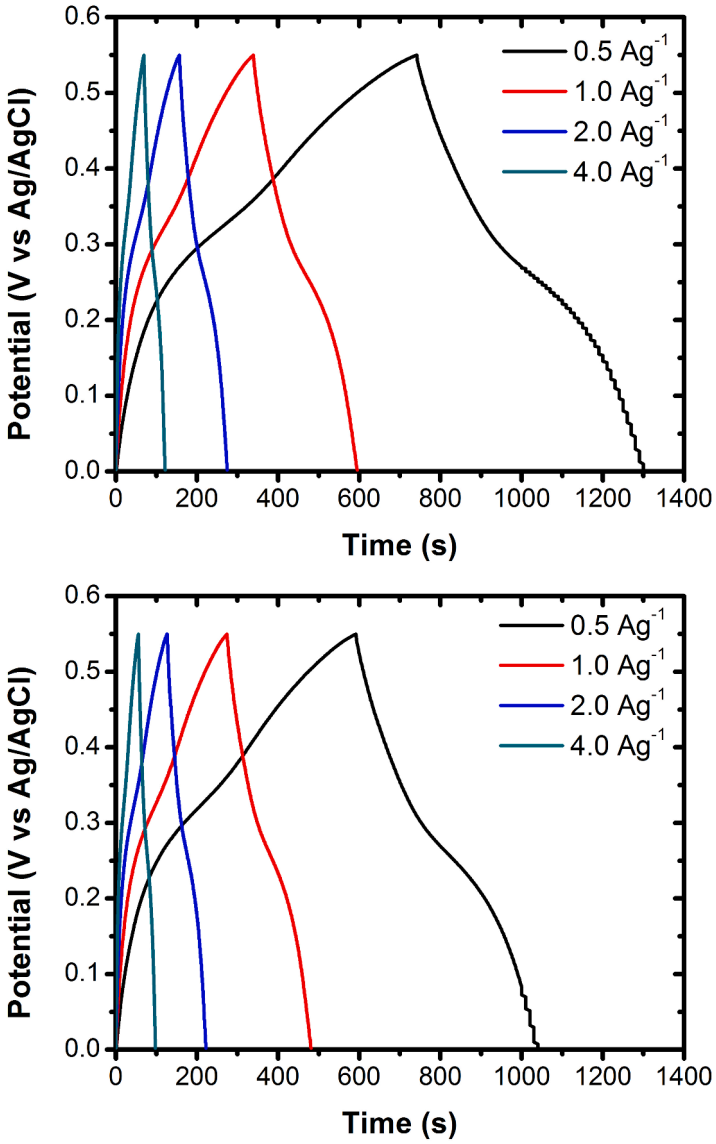

Fig. 9. (*continued*).

films were determined by using the equation [63].

$$C_s = \frac{I \times \Delta t}{m \times \Delta V} \tag{10}$$

$$SE = \tfrac{1}{2} C_s \times \Delta V^2 \tag{11}$$

$$SP = \frac{SE \times 3600}{t_d} \tag{12}$$

where, I is the constant applied current, ΔV is the change in voltage, m is the mass of the deposited film, and t_d is the discharge time. Fig. 10(b) shows the variation of specific capacitance with current density for $CoFe_2O_4$ thin films prepared by spray pyrolysis. The maximum specific capacitance was found to be 575 Fg^{-1} at a current density of 0.5 Ag^{-1} for the $CoFe_2O_4$ thin film prepared at 425 °C. This result is in good agreement with specific capacitance obtained from CV. $CoFe_2O_4$ thin film prepared at 425 °C showed better specific capacitance due to its terminal thickness and enhancement in the surface morphology. The observed specific capacitance is superior to value of 429 Fg^{-1} at a current density 0.5 Ag^{-1} reported by Kennaz et al. [24] for cobalt ferrite magnetic nanoparticles.

Fig. 10(c) shows the Ragone plot for $CoFe_2O_4$ thin film prepared at substrate temperature of 425 °C. The specific energy and specific power of $CoFe_2O_4$ thin film prepared at substrate temperature of 425 °C were found to be 17.86 $Whkg^{-1}$ and 1108 Wkg^{-1} respectively at current density of 4 Ag^{-1}. The determined specific energy and specific power of $CoFe_2O_4$ thin film prepared at substrate temperature of 425 °C at various current densities are mentioned in the Table 4. These values are superior to previously reported values by Gao and coworkers [62] for porous $CoFe_2O_4$ nanosheets. Fig. 10(d) shows the cycling performance of 1000 cycles at current density of $1Ag^{-1}$ for $CoFe_2O_4$ thin film prepared at substrate temperature of 425 °C. The inset of Fig. 10(d) shows the charge-discharge curves of initial ten cycles. The $CoFe_2O_4$ thin film prepared at substrate temperature of 425 °C exhibited 93.03% retention of its specific capacitance after continuous 1000 cycles at a current density of 1 Ag^{-1}.

3.8.3. EIS

The impedance spectra of $CoFe_2O_4$ thin films were recorded in the frequency range from 1 Hz to 100 kHz. Fig. 11 shows the Nyquist plot i. e., the real part (Z') versus the imaginary part (Z'') of complex impedance for $CoFe_2O_4$ thin film electrodes prepared by spray pyrolysis at various substrate temperatures. There is one prominent semi-circular arc for every sample in figure representing that the grain boundary

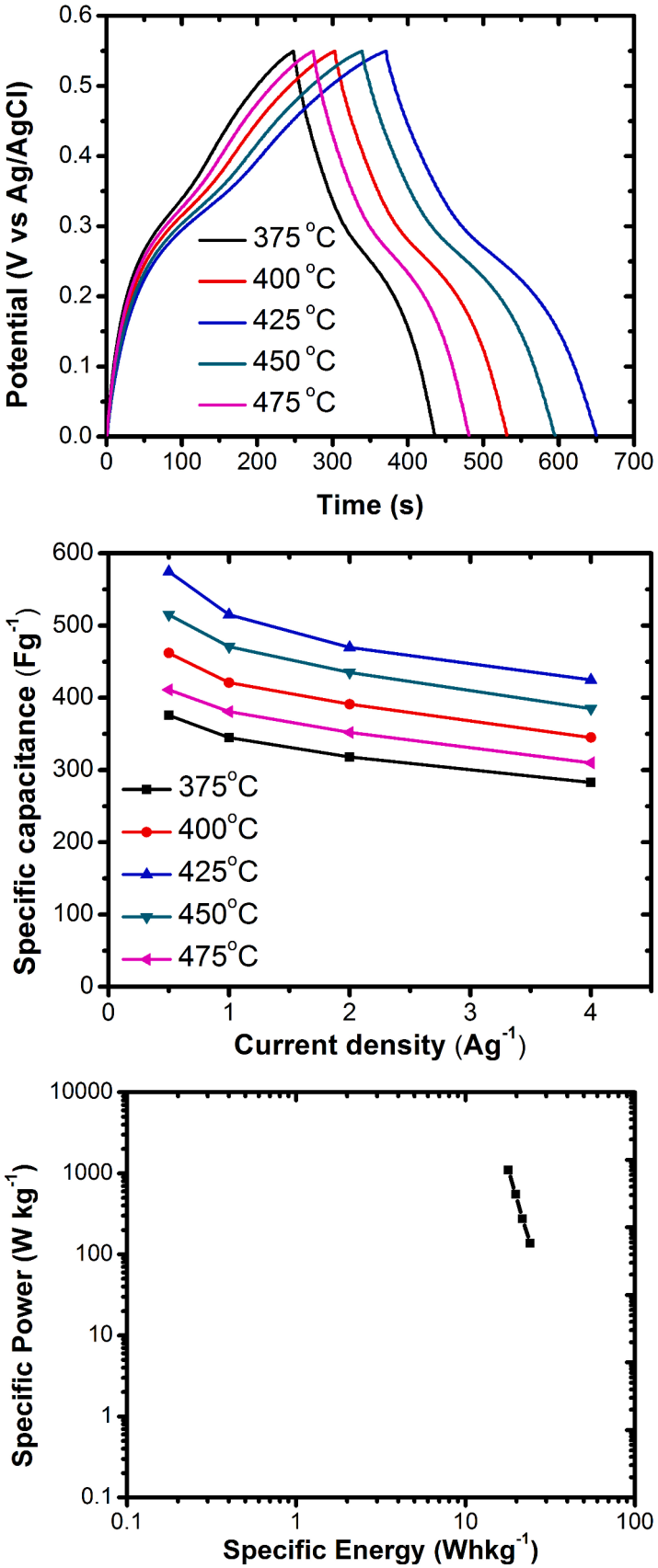

Fig. 10. (a) GCD curves at current density of 1 Ag^{-1} and (b) plot of specific capacitance versus current density for $CoFe_2O_4$ electrodes prepared by spray pyrolysis at various substrate temperatures; (c) Ragone plot of $CoFe_2O_4$ thin film electrode prepared at substrate temperature of 425 °C and (d) Long term cycling performance of the $CoFe_2O_4$ thin films spray deposited at substrate temperature of 425 °C and at the current density of 1 Ag^{-1}. The inset shows the charge-discharge curves of the first 10 cycles of the $CoFe_2O_4$ thin films.

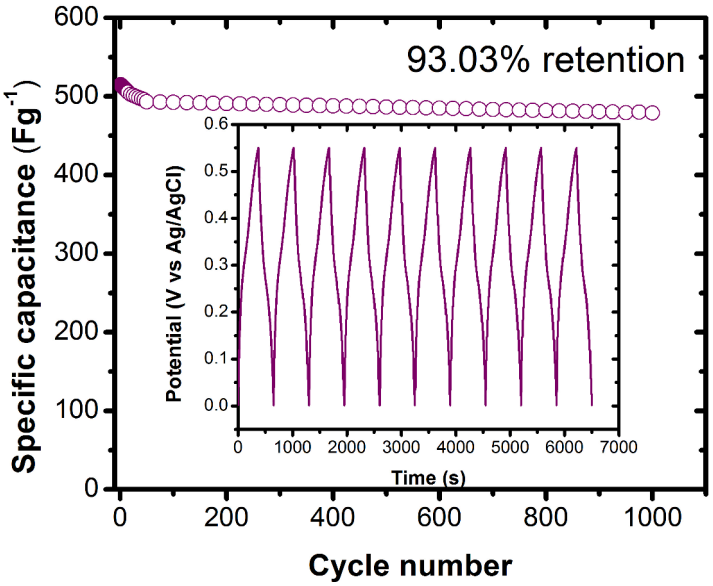

Fig. 10. (*continued*).

Table 4
The specific energy and specific power for $CoFe_2O_4$ electrodes prepared at substrate temperature of 425 °C.

Current density (Ag^{-1})	t_{dis} (*sec*)	SE ($Wh{\cdot}kg^{-1}$)	SP ($W{\cdot}kg^{-1}$)
0.5	632	24.16	138
1	283	21.64	275
2	129	19.75	551
4	58	17.86	1108

tdis; discharge time, SE; Specific energy, SP; Specific power.

conduction rules over the grain conduction [64]. The solution resistances (Rs) obtained for the $CoFe_2O_4$ thin film electrodes prepared by spray pyrolysis at various substrate temperatures are low and thin film prepared at 425 °C has the lowest solution resistance of 0.25 Ω. The diameter of semicircle represents the charge transfer resistance (Rct) at the electrode electrolyte interface. Table 5 shows the values of solution resistance (Rs) and charge transfer resistance (Rct) for $CoFe_2O_4$ thin film electrodes prepared by spray pyrolysis at various substrate temperatures. The lowest values Rs and Rct for $CoFe_2O_4$ thin film prepared at 425 °C showed better electrochemical behaviour which is in good agreement with results obtained from electrical resistivity.

4. Conclusions

$CoFe_2O_4$ thin films were prepared at various substrate temperatures via chemical spray pyrolysis method. The effects of substrate temperatures on the film properties were studied. XRD study confirmed spinel crystal structure symmetry of Fd3m space group with crystallite size in the range of 15 to 23 nm. FESEM showed the porous spherical grain like surface morphology. EDX study confirmed that the films are stoichiometric. Optical bandgap energy was observed in the range of 2.33 to 2.54 eV. The electrical resistivity measurement confirmed that films are semiconducting. $CoFe_2O_4$ thin film prepared at 425 °C showed maximum specific capacitance of 543 Fg^{-1} at scan rate of 5 mVs^{-1} from CV and 575 Fg^{-1} at current density of 0.5 Ag^{-1} from GCD with potential

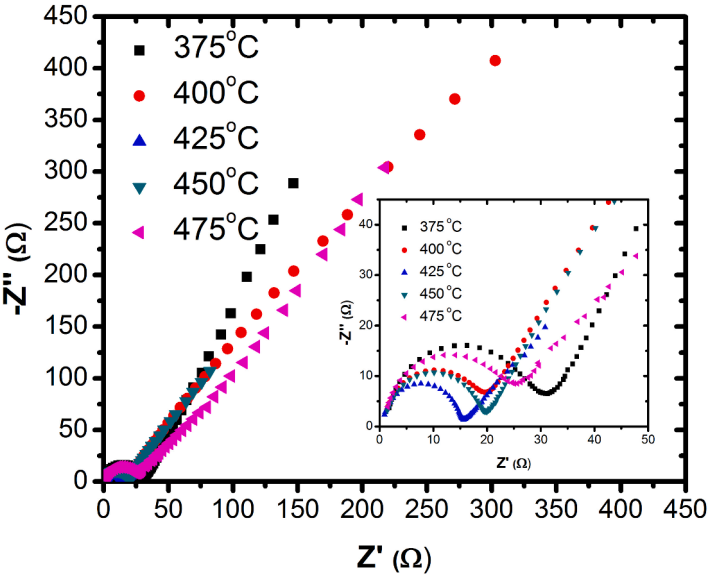

Fig. 11. : Nyquist plot for $CoFe_2O_4$ thin film electrodes prepared by spray pyrolysis at various substrate temperatures. The inset shows the enlarged Nyquist plot.

Table 5
Nyquist data for $CoFe_2O_4$ thin film electrodes prepared by spray pyrolysis at various substrate temperatures.

Substrate temperature (°C)	Rs (Ω)	Rct (Ωcm^2)
375	0.50	36.21
400	0.35	26.75
425	0.25	16.15
450	0.30	21.50
475	0.45	33.95

Rs; Solution resistance, Rct; Charge transfer resistance.

window of 0 V to 0.55 V. The specific energy and specific power of $CoFe_2O_4$ thin film prepared at 425 °C were found to be 17.86 $Whkg^{-1}$ and 1108 Wkg^{-1} respectively at current density of 4 Ag^{-1}. The specific capacitance of $CoFe_2O_4$ thin film electrode maintains 93.03% to its initial value after 1000 charge-discharge cycles, showed good cycling stability. The obtained results indicate that $CoFe_2O_4$ is one of the promising candidates for the future generation of energy storage device.

CRediT authorship contribution statement

Vidyadevi A. Jundale: Writing – original draft, Visualization, Investigation. **Abhijit A. Yadav:** Conceptualization, Methodology, Supervision, Writing – review & editing.

Declaration of Competing Interest

The authors declare that they have no known competing financial interests or personal relationships that could have appeared to influence the work reported in this paper.

Data availability

No data was used for the research described in the article.

References

[1] B. Huang, X. Wu, Dispersed nickel-cobalt double metal hydroxide self-assembled with polystyrene sulfonic acid polyelectrolyte for the preparation of carbon solid solid supercapacitors with wide temperature range and long cycle stability, Thin Solid Films 734 (2021), 138838.

[2] D.A. Oliveira, J.L. Lutkenhaus, J.R. Siqueira, Building up nanostructured layer-by-layer films combining reduced graphene oxide-manganese dioxide nanocomposite in supercapacitor electrodes, Thin Solid Films 718 (2021), 138483.

[3] K.K. Patel, T. Singhala, V. Pandey, T.P. Sumangala, M.S. Sreekanth, Evolution and recent developments of high performance electrode material for supercapacitors: a review, J. Ener. Storage 44 (2021), 103366.

[4] N. Hamzan, M.M. Ramly, M.F. Omar, H. Nakajima, S. Tunmee, S.A. Rahman, B. T. Goh, Optimized shell thickness of NiSi/SiC core-shell nanowires grown by hot-wire chemical vapour deposition for supercapacitor applications, Thin Solid Films 716 (2020), 138430.

[5] J.W.N. Júnior, R.M. Monção, R.M. Bandeira, J.R.S. Júnior, J.F.D.F. Araujo, J.V. B. Moura, L.B.S. Lima, F.E.P. Santos, C.L. Lima, T.H.C. Costa, Rômulo Ribeiro Magalhãesde Sousa, Growth of α-Fe_2O_3 thin films by plasma deposition: studies of structural, morphological, electrochemical, and thermal-optical properties, Thin Solid Films 736 (2021), 138919.

[6] R.K. Vishnu Prataap, R. Arunachalam, R.P. Raj, S. Mohan, L. Peter, Effect of electrodeposition modes on ruthenium oxide electrodes for supercapacitors, Curr. Appl. Phys. 18 (2018) 1143–1148.

[7] J.M. Kwon, J.-H. Kwon, J.-H. Kim, S.-H. Kang, C.-J. Choi, J.A. Rajesh, K.-S. Ahn, Facile hydrothermal synthesis of cubic spinel AB_2O_4 type $MnFe_2O_4$ nanocrystallites and their electrochemical performance, Appl. Surf. Sci. 413 (2017) 83–91.

[8] T. Dippong, E.A. Levei, O. Cadar, Recent Advances in Synthesis and Applications of MFe_2O_4 (M = Co, Cu, Mn, Ni, Zn) Nanoparticles, Nanomater 11 (2021) 1560.

[9] H. Xia, D. Zhu, Y. Fu, X. Wang, $CoFe_2O_4$-graphene nanocomposite as a high-capacity anode material for lithium-ion batteries, Electrochim. Acta 83 (2013) 166–174.

[10] G.A. El-Shobaky, A.M. Turky, N.Y. Mostafa, S.K. Mohamed, Effect of preparation conditions on physicochemical, surface and catalytic properties of cobalt ferrite prepared by coprecipitation, J. Alloys Compd. 493 (1–2) (2010) 415–422.

[11] J.S. Sagu, K.G.U. Wijayantha, A.A. Tahir, The Pseudocapacitive Nature of $CoFe_2O_4$ Thin Films, Electrochim. Acta 246 (2017) 870–878.

[12] S. Abbas, A. Munir, F. Zahra, M.A. Rehman, Enhanced electrical properties in Nd doped cobalt ferrite nano-particles, IOP Conf. Ser. 146 (2016), 012027.

[13] S. Anjum, G.H. Jaffar, A.K. Rumaiz, M.S. Rafique, S.I. Shah, Role of vacancies in transport and magnetic properties of nickel ferrite thin films, J. Phys. D 43 (2010), 265001.

[14] S.K. Kamilla, A. Kumar, Cobalt ferrite: a review, Mater. Today: Proceed. (2021), https://doi.org/10.1016/j.matpr.2021.03.687. In press.

[15] V.S. Kumbhar, A.D. Jagadale, N.M. Shinde, C.D. Lokhande, Chemical synthesis of spinel cobalt ferrite ($CoFe_2O_4$) nano-flakes for supercapacitor application, Appl. Surf. Sci. 259 (2012) 39–43.

[16] S.M. Nikam, A. Sharma, M. Rahaman, A.M. Teli, S.H. Mujawar, D.R.T. Zahn, P. S. Patil, S.C. Sahoo, G. Salvan, P.B. Patil, Pulsed laser deposited $CoFe_2O_4$ thin films as supercapacitor electrodes, RSC Adv. 10 (2020) 19353.

[17] A. Soam, R. Kumar, C. Mahender, M. Singh, D. Thatoi, R.O. Dusane, Development of paper-based flexible supercapacitor: bismuth ferrite/graphene nanocomposite as an active electrode material, J. Alloys Compd. 813 (2020), 152145.

[18] S.S. Raut, B.R. Sankapal, M.S.A. Hossain, S. Pradhan, R.R. Salunkhe, Y. Yamauchi, Zinc ferrite anchored multiwalled carbon nanotubes for high-performance supercapacitor applications, Eur. J. Inorg. Chem. (2018) 137–142.

[19] Li Gao, E. Han, Y. He, C. Du, J. Liu, Xu Yang, Effect of different templating agents on cobalt ferrite ($CoFe_2O_4$) nanomaterials for high-performance supercapacitor, Ionics (Kiel) 26 (2020) 3643–3654.

[20] B. Aspe, A. Malyeyev, A. Vakilinejad, K. Menguelti, A. Michels, N. Bahlawane, Chemical vapor deposition of $CoFe_2O_4$ micropillar arrays with enhanced magnetic properties, J. Alloys Compd. 890 (2022), 161758.

[21] S.D. Sartale, C.D. Lokhande, V. Ganesan, Electrochemical deposition and characterization of $CoFe_2O_4$ thin films, physica status solidi (a) 202 (2005) 85–94.

[22] H. Le Trong, T.M.A. Bui, L. Presmanes, A. Barnabé, I. Pasquet, C. Bonningue, P. H. Tailhades, Preparation of iron cobaltite thin films by RF magnetron sputtering, Thin Solid Films 589 (2015) 292–297.

[23] K. Maaz, A. Mumtaz, S.K. Hasanaina, Synthesis and magnetic properties of cobalt ferrite ($CoFe_2O_4$) nanoparticles prepared by wet chemical route, J. Magn. Magn. Mater. 308 (2007) 289–295.

[24] H. Kennaz, A. Harat, O. Guellati, D.Y. Momodu, F. Barzegar, J.K. Dangbegnon, N. Manyala, M. Guerioune, Synthesis and electrochemical investigation of spinel cobalt ferrite magnetic nanoparticles for supercapacitor application, J. Solid State Electrochem. 22 (3) (2018) 835–847.

[25] S.S. Bellad, C.H. Bhosale, Substrate temperature dependent properties of sprayed $CoFe_2O_4$ ferrite thin films, Thin Solid Films 322 (1–2) (1998) 93–97.

[26] A.A. Yadav, T.B. Deshmukh, R.V. Deshmukh, D.D. Patil, U.J. Chavan, Electrochemical supercapacitive performance of Hematite α-Fe_2O_3 thin films prepared by spray pyrolysis from non-aqueous medium, Thin Solid Films 616 (2016) 351–358.

[27] P. Shankar, P. Srinivasan, B. Vutukuri, A. Jayalath, G.K.M. Kulandaisamy, K. Jayanth Babu, J.H. Lee, J.B.B. Rayappan, Boron induced c-axis growth and ammonia sensing signatures of spray pyrolysis deposited ZnO thin films - relation between crystallinity and sensing, Thin Solid Films 746 (2022), 139126.

[28] L. Thirumalaisamy, N. Ahsan, K. Sivaperuman, M. Kim, S. Kunjithapatham, Y. Okada, Engineering of sub-band in $CuGaS_2$ thin films via Mo doping by chemical spray pyrolysis route, Thin Solid Films 709 (2020), 138252.

[29] N. Karthigayan, P. Manimuthu, M. Priya, S. Sagadevan, Synthesis and characterization of $NiFe_2O_4$, $CoFe_2O_4$ and $CuFe_2O_4$ thin films for anode material in Li-ion batteries, Nanomater. Nanotechnol. 7 (2017) 1–5.

[30] S.D. Sartale, C.D. Lokhande, Room temperature preparation of $NiFe_2O_4$ thin films by electrochemical route, Indian J. Eng. Mater. Sci. 7 (2000) 7404–7410.

[31] P.D. Thang, G. Rijnders, D.H.A. Blank, Spinel cobalt ferrite by complexometric synthesis, J. Magn. Magn. Mater. 295 (2005) 251–256.

[32] A.A. Yadav, U.J. Chavan, Influence of substrate temperature on electrochemical supercapacitive performance of spray deposited nickel oxide thin films, J. Electroanal. Chem. 782 (2016) 36–42.

[33] S. Gates-Rector, T. Blanton, The powder diffraction file: a quality materials characterization database, Powder Diffraction 34 (4) (2019) 352–360.

[34] A.A. Yadav, U.J. Chavan, Electrochemical supercapacitive performance of spray deposited Co_3O_4 thin film nanostructures, Electrochim. Acta 232 (2017) 370–376.

[35] B. Purnama, A.T. Wijayanta, Suharyana, Effect of calcination temperature on structural and magnetic properties in cobalt ferrite nano particles, J. King Saud Univ. – Sci. 31 (2019) 956–960.

[36] M. Sinha, A. Singh, R. Gupta, A.K. Yadav, M.H. Modi, Investigation of soft X-ray optical properties and their correlation with structural characteristics of zirconium oxide thin films, Thin Solid Films 721 (2021), 138552.

[37] S.R. Gibin, P. Sivagurunathan, Synthesis and characterization of nickel cobalt ferrite ($Ni_{1-x}Co_xFe_2O_4$) nano particles by co-precipitation method with citrate as chelating agent, J. Mater. Sci.: Mater. Electron 28 (2017) 1985–1996.

[38] R. Chandrashekhar, A.A. Yadav, Spray-deposited cobalt-doped RuO_2 electrodes for high-performance supercapacitors, Electrochim. Acta 437 (2023), 141521.

[39] X. Feng, Y. Huang, X. Chen, C. Wei, X. Zhang, M. Chen, Hierarchical $CoFe_2O_4$/$NiFe_2O_4$ nanocomposites with enhanced electrochemical capacitive properties, J. Mater. Sci. 53 (4) (2017) 2648–2657.

[40] W. Rao, Y.B. Wang, Y.A. Wang, J.X. Gao, W.L. Zhou, J. Yu, Surface Morphology and Magnetic Properties of $CoFe_2O_4$ Thin Films Prepared via Sol-Gel Method, Adv. Mat. Res. 750-752 (2013) 1024–1028.

[41] C.R. Chikkegowda, A.A. Yadav, Precursor solution concentration-dependent electrochemical supercapacitive behavior of spray-deposited RuO_2 films using aqueous/organic solvent mixtures, J. Appl. Electrochem. (2022), https://doi.org/10.1007/s10800-022-01806-7.

[42] A.A. Yadav, Spray deposition of tin oxide thin films for supercapacitor applications: effect of solution molarity, J. Mater. Sci.: Mater. Electron 7 (2016) 6985–6991.
[43] D. Yuliantika, A. Taufiq, A. Hidayat, N.H. Sunaryono, S. Soontaranon, Exploring structural properties of cobalt ferrite nanoparticles from natural sand, IOP Conf. Ser. 515 (2019), 012047.
[44] D. Sharma, N. Khare, Tuning of optical bandgap and magnetization of $CoFe_2O_4$ thin films, Appl. Phys. Lett. 105 (2014), 032404.
[45] N.T.T. Loan, N.T.H. Lan, N.T.T. Hang, N.Q. Hai, D.T.T. Anh, V.T. Hau, L.V. Tan, T. V. Tran, $CoFe_2O_4$ Nanomaterials: effect of annealing temperature on characterization, magnetic, photocatalytic, and photo-fenton properties, Processes 7 (12) (2019) 885.
[46] N. Kamarulzaman, M.F. Kasim, R. Rusdi, Band gap narrowing and widening of ZnO nanostructures and doped materials, Nanoscale Res. Lett. 10 (2015) 346.
[47] A.V. Ravindra, M. Chandrika, C. Rajesh, P. Kollu, S. Ju, S.D. Ramarao, Simple synthesis, structural and optical properties of cobalt ferrite nanoparticles, Eur. Phys. J. Plus 134 (6) (2019) 296.
[48] C. Zhang, S. Bhoyate, C. Zhao, P.K. Kaho, N. Kostoglou, C. Mitterer, S.J. Hinder, M. A. Baker, G. Constantinides, K. Polychronopoulou, C. Rebholz, R.K. Gupta, Electrodeposited nanostructured $CoFe_2O_4$ for overall water splitting and supercapacitor applications, Catalysts 9 (2019) 176.
[49] J.L. Gunjakar, A.M. More, V.R. Shinde, C.D. Lokhande, Synthesis of nanocrystalline nickel ferrite ($NiFe_2O_4$) thin films using low temperature modified chemical method, J. Alloys Compd. 465 (1–2) (2008) 468–473.
[50] Y.M. Lu, W.S. Hwang, J.S. Yang, Effects of substrate temperature on the resistivity of non-stoichiometric sputtered NiO films, Surf. Coat. Technol. 155 (2002) 231–235.
[51] I.H. Gul, A. Maqsood, Structural, magnetic and electrical properties of cobalt ferrites prepared by the sol-gel route, J. Alloys Compd. 465 (2008) 227–231.
[52] R.A. Reddy, K.R. Rao, B.R. Babu, G.K. Kumar, C. Rajesh, A. Chatterjee, N.K. Jyothi, Structural, electrical and magnetic properties of cobalt ferrite with Nd^{3+} doping, Rare Metals 41 (1) (2022) 240–245.
[53] A.R. Chavan, J.S. Kounsalye, R.R. Chilwar, S.B. Kale, K.M. Jadhav, Cu^{2+} substituted $NiFe_2O_4$ thin films via spray pyrolysis technique and their high frequency devices application, J. Alloys Compd. 769 (2018) 1132–1145.
[54] L. Lv, Q. Xu, R. Ding b, L. Qi, H. Wang, Chemical synthesis of mesoporous $CoFe_2O_4$ nanoparticles as promising bifunctional electrode materials for supercapacitors, Mater. Lett. 111 (2013) 35–38.
[55] A. Yavuz, N. Ozdemir, P.Y. Erdogan, H. Zengin, G. Zengin, M. Bedir, Effect of electrodeposition potential and time for nickel film generation from ionic liquid electrolytes for asymmetric supercapacitor production, Thin Solid Films 711 (2020), 138309.
[56] N. Kumar, A. Kumar, G.-M. Huang, W.-W. Wu, T.Y. Tseng, Facile synthesis of mesoporous $NiFe_2O_4$/CNTs nanocomposite cathode material for high performance asymmetric pseudocapacitors, Appl. Surf. Sci. 433 (2018) 1100–1112.
[57] K.V. Sankar, R.K. Selvan, D. Meyrick, Electrochemical performances of $CoFe_2O_4$ nanoparticles and a rGO based asymmetric supercapacitor, RSC Adv. 5 (2015) 99959–99967.
[58] J. Yan, U. Khoo, A. Sumboja, P.S. Lee, Facile coating of manganese oxide on tin oxide nanowires with high performance capacitive behavior, ACS Nano 4 (2010) 4247–4255.
[59] A.A. Yadav, U.J. Chavan, Electrochemical supercapacitive performance of spray deposited $NiSnO_3$ thin films, Thin Solid Films 634 (2017) 33–39.
[60] L. Liu, H. Zhang, Y. Mu, Y. Bai, Y. Wang, Binary cobalt ferrite nanomesh arrays as the advanced binder-free electrode for applications in oxygen evolution reaction and supercapacitors, J. Power Sources 327 (2016) 599–609.
[61] P. Xiong, H. Huang, X. Wang, Design and synthesis of ternary cobalt ferrite/graphene/polyaniline hierarchical nanocomposites for high-performance supercapacitors, J. Power Sources 245 (2014) 937–946.
[62] H. Gao, J. Xiang, Y. Cao, Hierarchically porous $CoFe_2O_4$ nanosheets supported on Ni foam with excellent electrochemical properties for asymmetric supercapacitors, Appl. Surf. Sci. 413 (2017) 351–359.
[63] B.E. Conway, Electrochemical Supercapacitors: Scientific Fundamentals and Technological Applications, Kluwer Academic, New York, 1999.
[64] F.S.M. Sinfrônio, P.Y.C. Santana, S.F.N. Coelho, F.C. Silva, A.S. de Menezes, S. K. Sharma, magnetic and structural properties of cobalt- and zinc-substituted nickel ferrite synthesized by microwave-assisted hydrothermal method, J. Elec. Mater. 46 (2017) 1145–1154.